Non-destructive Evaluation Of Power-Generation Steel Microstructure Changes Using Electromagnetic Sensors

J. Liu[a], L. Zhou[a], X.J. Hao[a], M. Strangwood[a], A. Peyton[b], P. F. Morris[c], C.L. Davis[a]

[a]School of Metallurgy & Materials, University of Birmingham, B15 2TT

[b]School of Electrical and Electronic Engineering, University of Manchester, Manchester, M13 9PL

[c]Swinden Technology Centre, Tata Steel Europe, Rotherham, S60 3AR

ABSTRACT

This paper presents results from a multi-frequency electromagnetic (EM) sensor used to characterise the microstructural changes in P9 and T22 power generation steels after tempering and elevated temperature service exposure. The EM sensor can detect the microstructural changes in both steels due to the corresponding relative permeability values increasing from 33 to 67 and then 133 for P9 during the tempering and the long service exposure respectively while for T22 the permeability changes from 61 to 75 and then 86, as well as the relatively small percentages of resistivity change. The changes in the relative permeability values have been qualitatively correlated to the changes in microstructural features, which affect the domain wall movements during the multi-frequency EM sensor tests. The real inductance value at low frequencies L_0 is particularly affected by differences in the relative permeability of the steels studied, which is found to increase exponentially with the L_0 values in the range studied.

Introduction

Microstructural changes during operation of elevated temperature power generation steels alter their properties and their remaining safe operating life (remnant life) [1]. Efficient operation of power generation plant requires the microstructural condition to be assessed during service. Currently the microstructural state is assessed using replicas of the surface or inferred from hardness measurements, both taken during shut down periods. Non-destructive evaluation (NDE) of microstructural changes in power plant steels during their service life is of interest to aid in the determination of safe remnant life. Amongst a wide range of NDE techniques available, magnetic/

electromagnetic (EM) methods are of particular interest in evaluation of ferromagnetic ferritic heat resistant steels. EM sensors can be used in a non-contact fashion (with stand-off distances of over 10 mm) and can survey through (non-magnetic non-conducting) coatings. Ferritic Cr-Mo alloy steels are commonly used for heavy section power plant components such as steam line pipes, boiler tubes and turbine rotors operating at temperatures from around 560 C to 630°C. Future operating temperatures may increase to 650°C in order to increase the thermal efficiency of power plant [2].

Cr-Mo-based creep-resisting steels, such as the 2.25Cr-1Mo, 9Cr and 12Cr families, are normalised, normalised and tempered, or quenched and tempered at service entry with their microstructures consisting of a tempered lath martensite (lath widths about 0.3-0.5 m) strengthened by alloy carbides [3]. During elevated temperature service (usually for tens of years) the microstructure evolves gradually by coarsening of the fine tempered martensite laths into broader ferrite laths, coarsening of the fine M2X carbides into larger, equilibrium M23C6 and/or M6C carbides and finally the formation of an equiaxed ferrite grain structure with grain growth and the concentration of coarser carbides on ferrite grain boundaries [3].

Multi-frequency EM sensors have proved sensitive to the change of ferrite/austenite fraction [4,5], shown using model alloys, in-situ analysis and modelling, and also decarburisation [6, 7] shown for high carbon steels, for on-line and off-line monitoring. Prototype EM sensors are being used for in-situ monitoring of steel processing [8]. The theory as to how the relative permeability and resistivity of a sample affects the multi-frequency EM response is presented elsewhere [9]. It has been reported that the microstructural changes in power plant steels e.g. 9Cr-1Mo[10, 11], 2.25Cr-1Mo[10] subjected to long tempering and 5Cr-0.5Mo [12] subjected to creep testing result in changes to their magnetic properties. Therefore, multi-frequency EM sensors should be able to detect the relative permeability and resistivity changes, resulting from microstructural changes in power plant steels during service at high temperatures. To assess the sensitivity of a multi-frequency EM sensor to changes in microstructure, the present work has studied the EM sensor response to P9 and T22 power generation steel samples representative of initial service entry and long-term exposure microstructures.

Experiments

The P9 and T22 steels studied were removed from a service after approximately 11 years at 520°C. Their chemical compositions are given in Table 1. Selected samples (approx. 70mm×15mm×7mm) were heat treated to simulate the service entry microstructure, i.e. tempered martensite/bainite by normalising at 950°C for 1 hour or 940 °C for 1 hour followed by air cooling to room temperature and then tempering at 760°C for 1 hour or 720°C for 1.5 hours for P9 and T22 respectively. As-normalised samples were also examined. The heat treatment conditions have been determined as per ASTM standards A335 (13) and A213 (14) as well as literature data [10, 15-18].

TABLE 1: Chemical composition (wt%) of the P9 and T22 steels studied

	Cr	Mo	C	Si	Mn	P	S
P9	8.40	0.97	0.12	0.52	0.44	0.006	0.010
T22	2.14	1.01	0.15	0.28	0.44	0.017	0.011

Metallographic samples were polished to 0.25 m and etched in Kallings reagent for P9 and 2% nital for T22. Scanning electron microscope (SEM) micrographs were obtained using a JEOL-6060. A four-point probe technique was employed to measure the resistivity of the steels with a direct current Cropico DO5000 microhmmeter at room temperature using cylindrical specimens of 4.95 mm in diameter and 50.0 mm in length.

A cylindrical EM sensor, similar to that used in [6], consisting of one exciting coil and one sensing coil both wound around an insulating tube of 5.5 mm and 6.5mm inner and outer diameters respectively was used. EM sensor tests were carried out on the same cylindrical specimens as for the resistivity measurements. The sensor was operated at 3V and a range of frequencies from 10Hz to 1MHz. Signals picked up by the sensing coil were recorded and processed by an Impedance Analyzer (Model S1260) made by Solartron Analytical measuring complex trans-impedance, from which mutual inductance was calculated.

Results and discussion

The microstructure of the as-normalised P9 consists of predominantly martensite mixed with some bainite as shown in Fig. 1(a). Subsequent tempering produces a simulated service entry microstructure, i.e. tempered martensite/bainite as shown in Fig. 1(b). After long service exposure, the microstructure showed equiaxed ferrite with large carbides distributed within ferrite grains or on grain boundaries as shown in Fig. 1(c).

The electrical resistivity measurements of all the samples are given in Table 2. The tempering heat treatment has resulted in a 7.49% resistivity drop compared to the as-normalised P9 value. In contrast, the ex-service resistivity decrease compared with the normalised and tempered value is only 0.46% despite the large microstructural changes as described above. This is due to the resistivity value being most affected by the change in dislocation density and elements (for example carbon) in solution between the as-normalised condition and tempered condition, with the service exposure resulting in little further change in these factors.

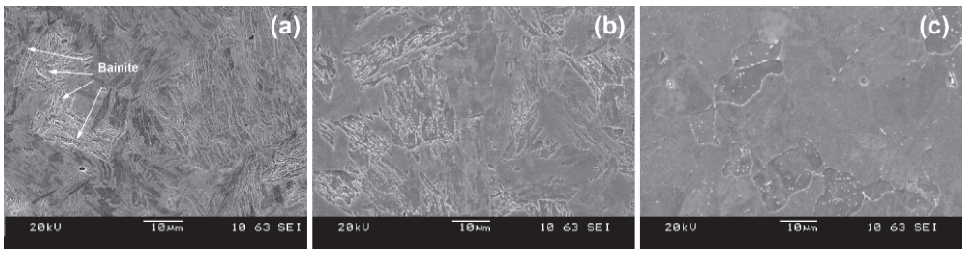

Fig. 1: Microstructure of the P9 samples in different conditions. (a) as normalized, (b) normalized and tempered and (c) ex-service.

Fig. 2 (a) show the EM sensor measurements of the P9 samples as the real part of mutual inductance as a function of frequency. The real inductance is essentially independent of frequency over the low frequency (approx 10 - 100Hz) range then drops continuously with increasing frequency until it approaches zero at very high frequencies (over approximately 0.1MHz). For conciseness, the inductance value at low frequencies (here taken as the mean value for the first 5 data points from 10 to 25Hz) has been used as a characteristic parameter L_0; the values of which are given in Table 2.

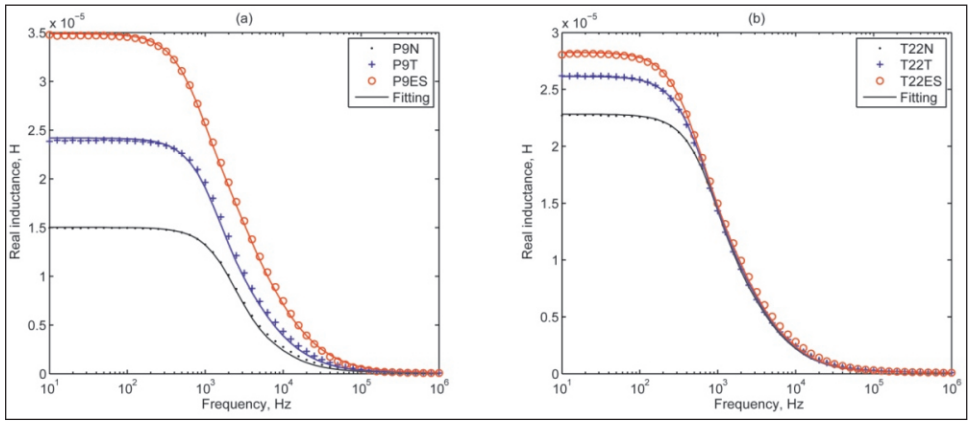

Fig. 2: Real and imaginary mutual inductance of EM sensor coils as a function of frequency for P9 and T22.

The L0 of the as-tempered P9 is 45% lower than that of the service exposed value and 37.5% higher than the as-normalised value. Over the low frequency range, the relative permeability dominates the L0 value as the eddy currents are insignificant. As the frequency increases eddy currents strengthen and reduce the mutual inductance, which accounts for the decreasing (damping) part of real inductance as shown in Fig. 2 (a).

Table 2: Measured resistivity, low frequency inductance values and fitted relative permeability values for P9 and T22 steels in different conditions

Sample	Electrical resistivity (10-7 ω m)	Real inductance at low frequencies L_O ($\times 10^{-5}$ H)	Fitted relative permeability
P9N	5.896 ± 0.008	1.4947 ± 0.0020	37
P9T	5.485 ± 0.003	2.3914 ± 0.0032	66
P9ES	5.460 ± 0.003	3.4655 ± 0.0058	133
T22N	3.337 ± 0.005	2.2691 ± 0.0057	61
T22T	2.833 ± 0.003	2.6114 ± 0.0111	75
T22ES	2.578 ± 0.002	2.8028 ± 0.0149	86

* Sample name suffixes N = as normalised, T = normalised and tempered, ES = ex-service;

A 2D axisymmetric finite element (FE) model was developed for modelling the sensor signal output in response to a steel sample of given resistivity and relative permeability using Comsol Multiphysics. The model is broadly similar to that described in [6]. The resistivity values of modelled samples were taken from the experimental measurements and the relative permeability values determined by fitting the modelled real inductance with the experimental measurement based on a non-linear least square method with 51 frequency points from 10Hz to 1MHz in Comsol LiveLink for Matlab. Close fits between the modelled and measured real inductance for all the samples have been achieved as shown in Fig. 2. The fitted relative permeability values are presented in Table 2 as well as plotted as a function of low frequency inductance values in Fig. 3. Fig. 3 indicates that the relative permeability values exponentially increase with corresponding low frequency inductance for both P9 and T22 steels in the different heat treated conditions.

During the service exposure for P9, when the resistivity change is negligible, the significant increase (>100%) in relative permeability can be attributed to the annihilation of the ferrite lath boundaries (formed of dislocation networks in tempered martensite) reducing the number of pinning points affecting domain wall motion. The increase in relative permeability during tempering for P9 can be ascribed to the change in microstructural features including a considerable decrease in the dislocation density in the strained martensite laths of the as-normalized P9, and as a result of changes in the laths to a larger lath size, as can be seen in Fig. 1(a) and (b). These factors are expected to have a more dominant effect than the precipitation of carbides occurring mostly on lath and prior austenite grain boundaries, which play a relatively minor role in pinning domain walls as the grain/lath boundaries appear to be the major pinning points in this case [19,20].

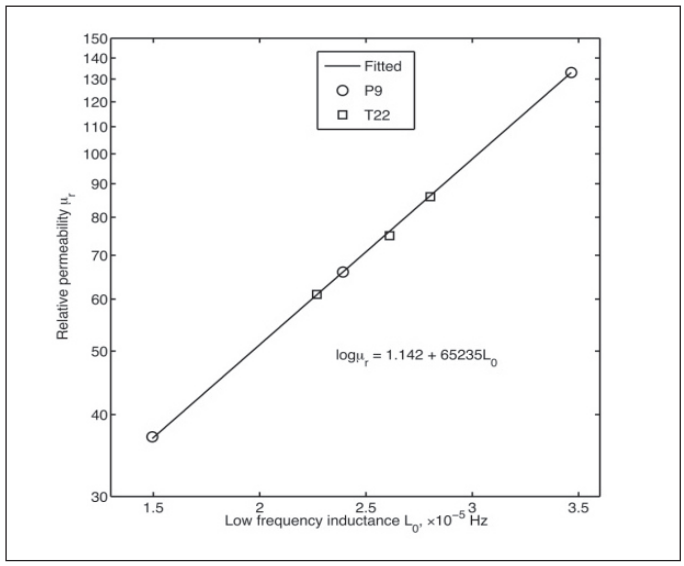

Fig. 3: Relative permeability as a function of low frequency inductance for both P9 and T22 samples in different conditions fitting well with an exponential relationship.

The as-normalised T22 steel shows a mixed microstructure of bainite and some proeutectoid ferrite as shown in Fig. 4(a). No carbides are present in the ferrite, but plate-like carbides can be seen within the bainite region. After tempering many carbides can be observed along prior austenite grain boundaries, on ferrite boundaries or within bainite regions as shown in Fig. 4(b). The microstructure of T22 after the service exposure consists of equiaxed ferrite and a great many carbides outlining the ferrite grain boundaries or finely dispersed within the ferrite grains as shown in Fig. 4(c).

Compared to P9 the T22 steel samples have much lower resistivity values due to a much lower content of solute alloy elements. However, the resistivity decrease due to service exposure and tempering are more significant than in P9, being 9.00% and 17.79% respectively.

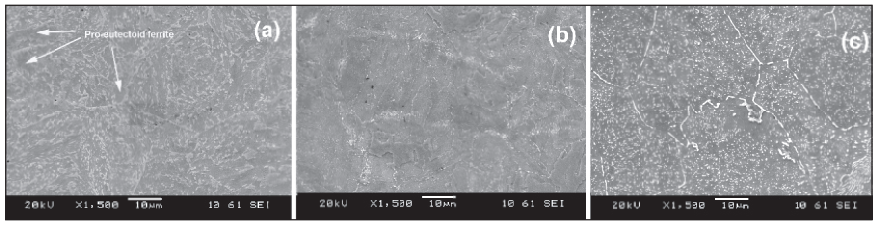

Fig. 4: Microstructure of the T22 samples in different conditions.
(a) as normalized, (b) normalized and tempered and (c) ex-service

The EM sensor measurements of the T22 samples in terms of the real part of mutual inductance as a function of frequency, is shown in Fig. 2 (c) and (d). The L_0 of the T22 changes on tempering and after service exposure in a similar manner as the P9 although to a lesser extent. There has been an 11.2% increase of L_0 after service and 13.1% after tempering, corresponding to a 14.7% and 23.0% increase in relative permeability after service and tempering respectively.

There should be very low mobile dislocation densities present in both the T22 and P9 samples after a long service exposure. In comparison with P9, the service exposed T22 has a much lower relative permeability although it has, on average, a larger ferrite grain size, which would be expected to permit more domain wall motion before encountering a grain boundary and hence a higher relative permeability. However the service exposed T22 appears to contain more carbide precipitates that provide pinning points for domain wall motion. This may be due to their fine dispersion within the grains giving rise to a shorter mean free path for domain wall motion (the precise role of carbides on pinning domain wall motion will depend on their type, size, number and distribution, this requires further study). This outweighs the difference in ferrite grain size and accounts for the lower relative permeability value. The as-tempered T22 has a slightly higher relative permeability value compared with the as-tempered P9, which can be attributed to a slightly larger lath size in T22 and a similar distribution of carbides, that is, mainly on lath and prior austenite grain boundaries as well as being comparable in number as can be observed in Fig. 1(b) and Fig. 3(b). For the normalised condition, the higher relative permeability value for the T22 is as expected from the higher proportion of bainite consisting of ferrite laths with carbides present (and proeutectoid ferrite, which is known to have a higher permeability [6,7]) rather than the strained martensite laths with a high dislocation density present in the as-normalised P9.

Conclusion

In conclusion, the present multi-frequency EM sensor has proved sensitive to relatively small microstructural changes in both P9 and T22 steels during tempering and service that can be related to the changes in their resistivity and relative permeability. The real inductance at low frequencies L_0 is particularly affected by differences in the relative permeability of the steels studied, which is found to increase exponentially with the L_0 values in the range studied.

Acknowledgement

This work was carried out with financial support from EPSRC under the grant EP/H023429/1.

References

1. B. Raj, V. Moorthy, T. Jayakumar, K.B.S. Rao, Int Mater Rev, 48 (2003) 273-325.
2. F. Masuyama, ISIJ Int, 41 (2001) 612-625.
3. P. Ennis, A. Czyrska-Filemonowicz, SADHANA-Acad P Eng S, 28 (2003) 709-730.
4. W. Yin, X.J. Hao, A.J. Peyton, M. Strangwood, C.L. Davis, NDT & E Int, 42 (2009) 64-68.
5. S.J. Dickinson, R. Binns, W. Yin, C. Davis, A.J. Peyton, IEEE T Instruments, 56 (2007) 879-886.
6. X. Hao, W. Yin, M. Strangwood, A. Peyton, P. Morris, C. Davis, Metall Mater Trans A, 40 (2009) 745-756.
7. X.J. Hao, W. Yin, M. Strangwood, A.J. Peyton, P.F. Morris, C.L. Davis, Scripta Mater, 58 (2008) 1033-1036.
8. A.J. Peyton, W. Yin, S.J. Dickinson, C.L. Davis, M. Strangwood, X. Hao, A.J. Douglas, P.F. Morris, Ironmaking Steelmaking, 37 (2010) 135-139.
9. R.J. Haldane, W. Yin, M. Strangwood, A.J. Peyton, C.L. Davis, Scripta Mater, 54 (2006) 1761-1765.
10. V. Moorthy, S. Vaidyanathan, B. Raj, T. Jayakumar, B. Kashyap, Metsll Mater Trans A, 31 (2000) 1053-1065.
11. A. Mitra, J.N. Mohapatra, J. Swaminathan, M. Ghosh, A.K. Panda, R.N. Ghosh, Scripta Mater, 57 (2007) 813-816.
12. J.N. Mohapatra, N.R. Bandyopadhyay, M.K. Gunjan, A. Mitra, J Magn Magn Mater, 322 (2010) 589-595.
13. ASTM standards A335/A335M -09a, 2009
14. ASTM standards A213/A213M - 09b, 2009
15. S. Saroja, M. Vijayalakshmi, V.S. Raghunathan, Mater T JIM, 34 (1993) 901-906.
16. B. Arivazhagan, R. Prabhu, S. Albert, M. Kamaraj, S. Sundaresan, J Mater Eng PERFORM, 18 (2009) 999-1004.
17. J.R. Yang, C.Y. Huang, C.N. Yang, J.L. Horng, Mater Charact, 30 (1993) 75-88.
18. G. Sangdahl, M. Semchyshen, Application of 2¼Cr-1 Mo Steel for Thick-Wall Pressure Vessels, ASTM 1982.
19. A.D. Beale, J.P. Jakubovics, M.G. Hetherington, C.B. Scruby, B.A. Lewis, K.J. Davies, J Magn Magn Mater, 104-107 (1992) 365-367.
20. J.A. Baldwin Jr, P.W. Smith Jr, F. Milstein, Sold State Commun, 17 (1975) 973-974.